Loughborough University

This item was submitted to Loughborough's Research Repository by the author.
Items in Figshare are protected by copyright, with all rights reserved, unless otherwise indicated.

A 10 GW Tesla-driven Blumlei pulsed power generator

PLEASE CITE THE PUBLISHED VERSION

http://dx.doi.org/10.1109/TPS.2014.2317572

PUBLISHER

© IEEE

VERSION

AM (Accepted Manuscript)

PUBLISHER STATEMENT

This work is made available according to the conditions of the Creative Commons Attribution-NonCommercial-NoDerivatives 4.0 International (CC BY-NC-ND 4.0) licence. Full details of this licence are available at: https://creativecommons.org/licenses/by-nc-nd/4.0/

LICENCE

CC BY-NC-ND 4.0

REPOSITORY RECORD

Novac, Bucur M., Meng Wang, Ivor R. Smith, and Peter Senior. 2019. “A 10 GW Tesla-driven Blumlei Pulsed Power Generator”. figshare. https://hdl.handle.net/2134/20451.

A 10 GW TESLA-DRIVEN BLUMLEIN PULSED POWER GENERATOR

Bucur M. Novac, *Senior Member, IEEE,* Meng Wang, *Student Member, IEEE,* Ivor R. Smith, *Senior Member, IEEE* and Peter Senior

***Abstract*— A repetitive 0.6 MV, 10 GW Tesla-driven Blumlein pulsed power generator, with an overall energy efficiency in excess of 90%, has been designed, manufactured and demonstrated by the Pulsed Power Group at Loughborough University. The paper describes the application of various numerical techniques used to design a successful generator, such as filamentary modelling and electrostatic and transient circuit analysis. All the major parameters of both the Tesla transformer and the Blumlein pulse forming line were determined, enabling accurate modelling of the overall unit to be performed. The wide-bandwidth embedded sensors used to monitor the dynamic characteristics of the overall system are also presented. Experimental results obtained during this major experimental program are compared with theoretical predictions and the way ahead towards generating faster output voltage impulses is considered.**

Index*— *Tesla transformers, Blumlein pulse forming line, high-voltage, switches

I. INTRODUCTION

A broad range of modern pulsed power applications, including plasma physics, lasers, particle accelerators, aeronautics, outer space science, food industry PEF sterilization, bioelectric studies, medical cancer treatment and the defense industry all require the generation of very fast high-voltage pulses. Marx generators can conveniently be used for this purpose, but Tesla transformers are also used in the construction of high-power microwave generators, electron beam sources, lasers and powerful ultra-wide-band radiation sources. In these latter applications, the Tesla transformer is used to charge a pulse forming line (*PFL*), or better a Blumlein pulse forming line (*B-PFL*), that is subsequently discharged into a load via a peaking closing switch or an additional bipolar pulse forming line.

The principles of both Tesla transformers and *B-PFL* generators are well-known, but the techniques used in their design are not adequately described. Fig. 1 shows a simplified Tesla transformer equivalent lumped circuit representation, where subscripts *P* and *S* denote respectively the total inductance *L*, capacitance *C* and resistance *R* of the primary and secondary circuits. *M* the mutual inductance between the coupled windings $M = k\sqrt{L_p L_s}$, where *k* is the magnetic coupling coefficient. An approximate analytical solution of the time dependence of the secondary (capacitive load) voltage following closure of the primary circuit switch is [1]:

B.M. Novac, Meng Wang, I.R. Smith and P. Senior are with the School of Electronic, Electrical and Systems Engineering, Loughborough University, Loughborough, Leicestershire LE11 3UE, UK (e-mail: B.M.Novac@lboro.ac.uk).

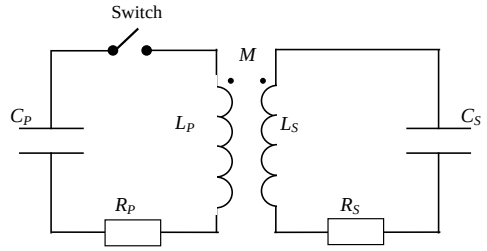


Fig. 1. Simplified lumped circuit representation of a Tesla transformer

$$V_S(t) \approx \frac{V_0}{2}\sqrt{\frac{L_S}{L_P}}\exp\left(-\frac{t}{\tau}\right)\left[\cos\left(\frac{\omega_r t}{\sqrt{1-k}}\right)-\cos\left(\frac{\omega_r t}{\sqrt{1+k}}\right)\right] \qquad (1)$$

where V_0 is the initial charging voltage of the capacitor C_p, $\tau = \frac{4 Q_P Q_S (1-k^2)}{\omega_r (Q_P + Q_S)}$ is the damping time constant, $Q_P = \frac{\omega_r L_P}{R_P}$ and $Q_S = \frac{\omega_r L_S}{R_S}$ are the quality factors (*Q*) of the primary and secondary winding circuits. The uncoupled resonant frequencies of these circuits are both equal, so that:

$$\frac{1}{\sqrt{L_P C_P}} = \frac{1}{\sqrt{L_S C_S}} = \omega_r \qquad (2)$$

Eq. (1) is reasonably accurate for values of the magnetic coupling $k < 0.6$ and *Q* factors greater than 10 (i.e., low resistance values for both R_p and R_s) and is often cited in reference to the design of Tesla transformers. The problem is that the techniques used to calculate accurately the various parameters in Eq. (1) are not usually presented. The first two sections of the present paper therefore introduce techniques useful for this purpose for both Tesla and *B-PFL* units. The two sections that then follow are devoted to the overall system design and to analyzing the results obtained with a *B-PFL* matched resistor attached to the output of the generator. The paper ends with conclusions and a presentation of the way ahead.

II. Calculation of Tesla Transformer Parameters

A. Calculation of Dynamic Resistance and Self and Mutual Inductance

The filamentary technique has been developed and applied at Loughborough for a broad range of pulsed power applications, with the way that it is used to calculate the Tesla transformer parameters being detailed in [2]. As Fig. 2 shows, the transformer is represented by a large collection of circular current filaments, for each of which a set of first order differential equations is written and solved. Solution of these equations not only provides values of the primary and secondary self-inductances and the mutual inductance between the windings, but also predicts the time history of all the currents in the system and their spatial distribution within conductors following a switching operation. It also provides a complete 2D mapping of both the magnetic and electric fields at any time throughout any operating conditions, the time-variation of resistance due to proximity and skin effects, the Joule energy deposited in the various conductors and their temperature distribution, as well as the forces acting between them. For the present Tesla design, the numerical modelling used the following input data for the two windings

- *primary single-turn coil*: inner radius, 170 mm; axial length, 150 mm; thickness, 0.1 mm

- *secondary helical coil*: inner radii along the plastic conical former, maximum 150 mm and minimum 91 mm; axial length, 180 mm; 30 turns of round conductor diameter, 1.2 mm, mounted in a helical groove in a former with an axial pitch of 6 mm (Fig. 3).

For the single-turn primary winding, the number of filaments was progressively increased according to the procedure outlined in [2], until the resulting numerical simulation for self-inductance reached an asymptote (converged) i.e., for a further substantial increase the result changed by less than 0.1%. A convenient filamentary representation of the primary is using a matrix of 5 (radially distributed) by 200 filaments (axially distributed). It is important to note that, due to skin effect, only an inner layer of 65 µm deep was actually considered in the filamentary representation.

The secondary winding was represented simply by a collection of 30 filamentary rings, although a more accurate representation is possible, in which each ring is further decomposed into a large number of filaments, to highlight both skin and proximity effects [3]. Analysis of the secondary circuit shows that the resistance of the helical coil does not play an important role and therefore in the present case the simplest filamentary representation was adopted, with the skin and proximity contributions to the overall secondary winding resistance being estimated using well-known formulae [4].

In reference to Fig. 1, the inductances calculated at the beginning of the capacitor discharge are: $L_P = 374.9$ nH, $L_S = 177$ µH and $M = 4.86$ µH, resulting in a magnetic coupling coefficient $k = 0.6$ (precisely the value required by the dual resonant conditions) and an ideal voltage

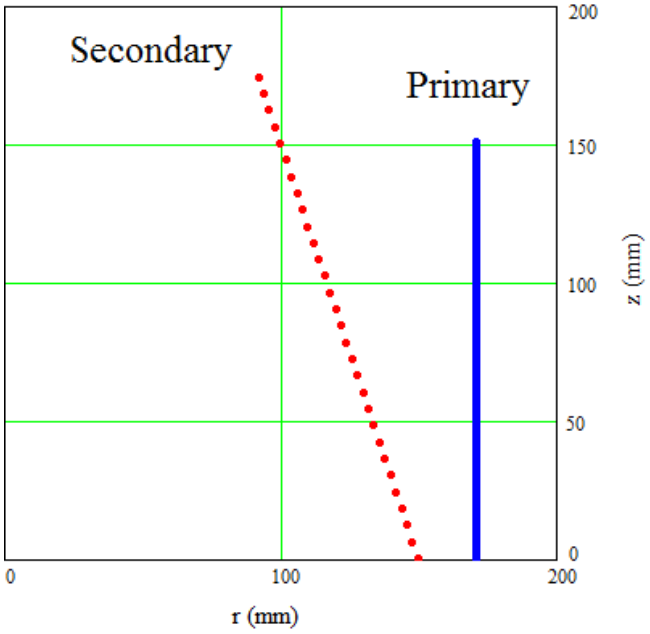


Fig. 2. 2D filamentary representation of the Tesla transformer in cylindrical geometry (due to symmetry, only half of the transformer is shown)



Fig. 3. Tesla transformer secondary winding

multiplication factor $k_V = \sqrt{\frac{L_S}{L_P}} \approx 22$.

The calculated resistances, also at the beginning of the capacitor discharge, are $R^0_{pw} \approx 1.78$ mΩ and $R^0_s \approx 2.5\ \Omega$ for the primary and secondary winding respectively.

The above lump parameters are used later as input data in calculations using PSpice software. During a shot, both the primary winding inductance and resistance vary as the current distribution in the cross-section of the single-turn changes slightly. The results provided by the filamentary model, which takes this fully into account, are considered therefore to be slightly more accurate.

B. Calculation of Secondary Winding Capacitance

The secondary winding capacitance of a Tesla transformer is a very important feature, but unfortunately little literature is published on ways by which it can be calculated. However, using the above filamentary representation of the helical secondary winding, the Maxwell matrix (termed ***B***) related to the capacitance network of the rings can be obtained using an electrostatic solver such as Maxwell SV [5]. The solver also provides the distribution of the electric field strength, essential in the analysis provided later for any electrical breakdown issues (Fig. 4). By adapting an existing technique [6] and using the matrix ***B***, the analysis and the corresponding procedure used to calculate the equivalent capacitance of the secondary winding are both detailed below. The ring capacitances form the equivalent complex lumped network presented in Fig. 5(a). This system of *N+1* conductors (*0,1,…,N*), with conductor *0* chosen as 'ground' or common reference will have *N* equations for the charges Q_i, with *i=1,...,N*, situated on the remainder of the conductors. In compact matrix representation, the equation takes the form:

$$Q_i = \sum_{j=1}^{N} B_{i,j} V_j^0 \tag{3}$$

where V_j^0 is the potential of conductor *j* with respect to conductor *0*.

For *i=j*, the terms $B_{i,i}$ are the Maxwell coefficients of self-capacitance C_i thus

$$C_i = B_{i,i} \tag{4}$$

defined as the charge to potential ratio on the *i*-th conductor when all the other conductors are grounded. Since the potential has the same sign as the charge, the coefficients $B_{i,i}$ are always positive.

For $i \neq j$ the terms $B_{i,j}$ are the Maxwell coefficients of induction and represent the partial capacitance or the negative of mutual capacitance $C_{i,j}$ between conductors *i* and *j* thus

$$C_{i,j} = -B_{i,j} = -B_{j,i} \tag{5}$$

calculated as the ratio of the induced charge on the *i*-th conductor to that of the potential of the *j*-th conductor, when all other conductors are grounded. The induced charge is always opposite in sign to the inducing charge, so $B_{i,j}$ is either negative or zero. Finally, the partial capacitance $C_{0,i}$ of the common reference conductor *0* with any other conductor *i* can be expressed as:

$$C_{0,i} = \sum_{k=1}^{N} B_{i,k} \tag{6}$$

In expanded matrix from, Eq. (3) can be re-written as:

$$\begin{pmatrix} Q^x \\ Q^y \end{pmatrix} = \begin{pmatrix} D^{xx} & D^{xy} \\ D^{yx} & D^{yy} \end{pmatrix} \cdot \begin{pmatrix} V^x \\ V^y \end{pmatrix} \tag{7}$$

where:

$$Q^x = \begin{pmatrix} Q_1 \\ Q_N \end{pmatrix}; Q^y = \begin{pmatrix} Q_2 \\ . \\ . \\ . \\ Q_{N-1} \end{pmatrix}; V^x = \begin{pmatrix} V_1 \\ V_N \end{pmatrix}; V^y = \begin{pmatrix} V_2 \\ . \\ . \\ . \\ V_{N-1} \end{pmatrix} \tag{8}$$

and

$$D^{xx} = \begin{pmatrix} B_{1,1} & B_{1,N} \\ B_{N,1} & B_{N,N} \end{pmatrix}; D^{xy} = \begin{pmatrix} B_{1,2} \ldots B_{1,N-1} \\ B_{N,2} \ldots B_{N,N-1} \end{pmatrix}; D^{yx} = \begin{pmatrix} B_{2,1} & B_{2,N} \\ \ldots\ldots\ldots\ldots & \\ B_{N-1,1} & B_{N-1,N} \end{pmatrix}; D^{yy} = \begin{pmatrix} B_{2,2} \ldots B_{2,N-1} \\ \ldots\ldots\ldots\ldots \\ B_{N-1,2} \ldots B_{N-1,N-1} \end{pmatrix} \tag{9}$$

The aim of the technique is to reduce the system of *N* capacitances in Fig. 5(a) to a system that has only one equivalent series capacitance and two parallel capacitances to ground, one for the system input and one for the output as shown in Fig. 5(b). To perform this transformation, all capacitances from *2* to *N* must simply be removed from the circuit. A simple way of achieving this is to ensure that they are not charged i.e., all charges Q_i (with *i=2,…N-1*) forced to be zero. This condition can be written in compact matrix form as $Q^y=0$, and introducing this into Eq. (7) enables firstly V^y to be found from:

$$V^y = -\left(D^{yy}\right)^{-1} D^{yx} V^x \tag{10}$$

and by re-introducing V^y back into Eq. (7), the matrix Q^x is obtained as:

$$Q^x = \left(D^{xx} - D^{xy}\left(D^{yy}\right)^{-1} D^{yx}\right) V^x = B^x V^x \tag{11}$$

where B^x is a four-element matrix given by:

$$B^x = D^{xx} - D^{xy}\left(D^{yy}\right)^{-1} D^{yx} \tag{12}$$

and contains the Maxwell coefficients for the new and simpler system of capacitances of Fig. 5(b). Finally, the new equivalent series capacitance placed between the system input and output is calculated using Eq. (5) as:

$$C_{in,out} = -B_{1,2}^x = -B_{2,1}^x \tag{13}$$

and the new partial capacitances with respect to ground, at the input and output, are obtained respectively using Eq. (6) as:

$$C_{ground,in} = B_{1,1}^x - B_{1,2}^x \tag{14}$$

$$C_{ground,out} = -B_{2,1}^x + B_{2,2}^x \tag{15}$$

When this technique is applied to the ***B*** matrix of the present Tesla transformer (the entire matrix is presented in [7]), the results obtained are: $C_{in,out}$ = 2.05 pF, $C_{ground,in}$ = 12.87 pF and $C_{ground,out}$ = 32.97 pF and the corresponding simplified lumped circuit representation of the secondary winding becomes as shown in Fig. 5(c). In the practical arrangement the input ('*in*' in Fig. 5(c)) is *directly connected* to the bank ground and therefore all three capacitances are in parallel with the two *B-PFL* capacitances (during charging, the *B-PFL* can be represented as a collection of two identical, parallel-connected capacitors), with all five being represented in Fig. 1 by a single capacitance C_s.

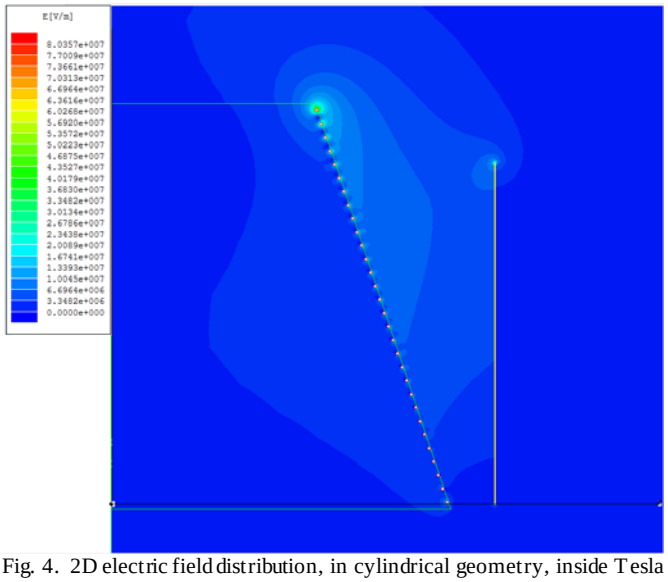


Fig. 4. 2D electric field distribution, in cylindrical geometry, inside Tesla transformer for a secondary voltage of 600 kV (due to symmetry, only half of the transformer is shown)

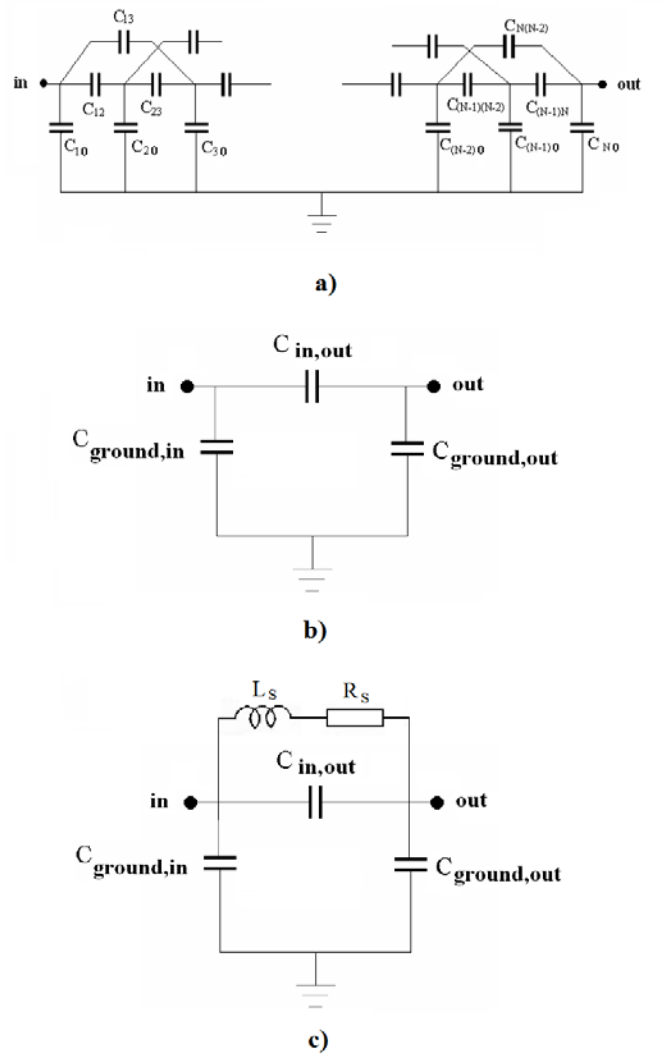


Fig. 5. (a) Secondary winding capacitance network (N=29);(b) simplified equivalent capacitances; (c) simplified representation of the secondary winding circuit

III. DESIGN AND CALCULATION OF BLUMLEIN PFL PARAMETERS

The *B-PFL* consists of a $l = 1$ m long, oil-filled, double-coaxial cylindrical geometry, having an inner electrode with an outer radius $r_1 = 104$ mm, an intermediate electrode with an outer radius $r_2 = 152.5$ mm and an outer electrode with an internal radius $r_3 = 222.25$ mm. Both the intermediate and the inner electrodes are steel cylinders with a wall thickness of $\delta = 1.5$ mm. It is straightforward to determine using the formula $Z_0 = \frac{ln(b/a)}{2\pi\varepsilon_0 c\sqrt{\varepsilon_{oil}}}$, where a and b are the inner and the outer radius of a coaxial transmission line, ε_0 is the permittivity of vacuum, $\varepsilon_{oil} \approx 2.25$ is the oil relative permittivity and c is the speed of light, that the resulting characteristic impedance of both of the two transmission lines so formed is $Z_0 \approx 15\ \Omega$. The velocity of the voltage impulse is given by $v = \frac{c}{\sqrt{\varepsilon_{oil}}} \approx 2 \cdot 10^8$ m/s, resulting in a duration of the load impulse $t_{B\text{-}PFL} = \frac{2l}{v} \approx 10\ ns$. Maxwell SV software was used to highlight possible dangers arising from the existence of regions of high electric field in the *B-PFL*. The design of the three electrodes (Fig. 6) was a tedious process, mainly related to finding the optimum diameter and position of the electric grading ring attached to the inner HV electrode in respect to a recess in the outer surface of that electrode (Fig. 6c). The final geometry electrode (Fig. 6a) produced an electric field distribution with a peak electric field strength of 223 kV/cm, for the *B-PFL* charged to 600 kV, which represents a substantial reduction from the peak field of 305 kV/cm generated by the commonly used and simpler geometry of Fig. 6(b). The breakdown electric field can be estimated using the Charlie Martin formula for oil under HV impulse [8]: $E_b = 480 \cdot t^{-1/3} A^{-0.067}\ kV/cm$, where t is the time in microseconds for which the instantaneous voltage exceeds 60% of the peak applied voltage and A is the surface area of the electrode in cm^2. Application of this formula, with $t \approx 0.4$ µs, to the outer surface of the inner electrode, for which $A \approx 6540$ cm^2, predicts there is a 50% chance of breakdown at an electric stress of $E_b \approx 360$ kV/cm. If this value is compared with the maximum electric stress inside the present *B-PFL* provided by the Maxwell software, the conclusion is that the oil is stressed up to 62% of the predicted breakdown value. The probability of failure can be more accurately predicted using the formula [9]: $PF = \frac{1}{2}\left(\frac{E_{max}}{E_b}\right)^{\frac{1}{0.067}}$, where E_{max} is the maximum applied electric field in kV/cm. For $E_{max} \approx 223$ kV/cm the resulting value $PF \approx 3.6 \cdot 10^{-4} \approx \frac{1}{2760}$ can be interpreted that if charged to 600 kV, a failure will only occur inside the *B-PFL* once in every 2760 shots. The two capacitances of the *B-PFL* were also obtained using Maxwell SV software as 341.3 pF for the

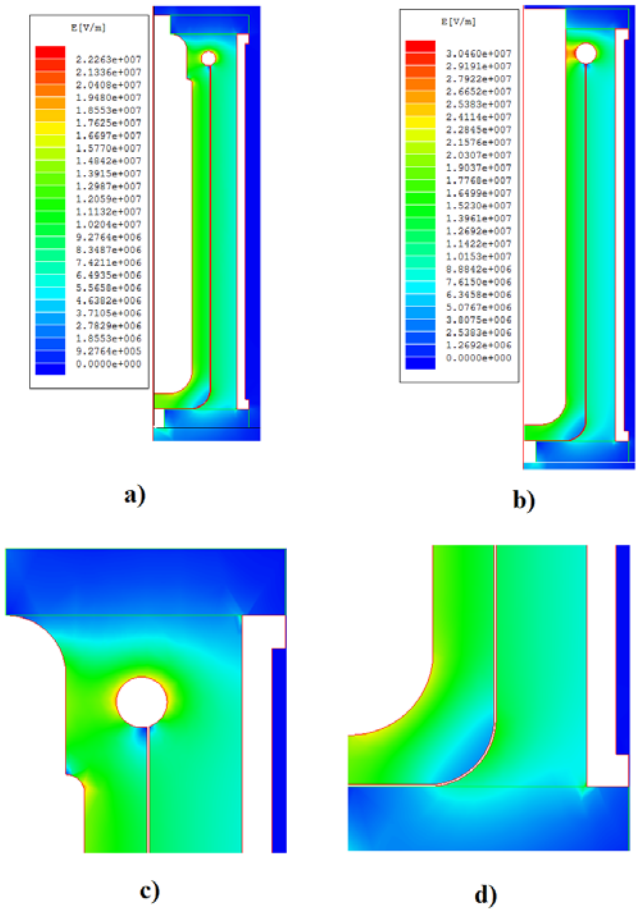


Fig. 6. 2D electric field distribution inside *B-PFL* at 600 kV
(a) for the present design, the maximum field strength is 223 kV/cm
(b) for a much simpler design, the maximum field strength is 305 kV/cm
(c) and (d) details near the electric grading elements for the design in (a)

outer and 326.5 pF for the inner PFL, resulting in an overall equivalent capacitance $C_{B\text{-}PFL} = 667.8$ pF. This enables the equivalent capacitance of the secondary winding circuit of the Tesla transformer to be determined as

$$C_S = C_{B-PFL} + C_{in,out} + C_{ground,in} + C_{ground,out} \approx 715\ pF$$

and its natural resonant frequency as 447 kHz.

IV. Overall Design and Manufacture, Diagnostics and Pspice Modeling

The overall layout is shown in Fig. 7, together with a photograph of the completed unit, including the frame which allows the generator to be easily moved. The overall dimensions and volume of the entire system, including the capacitor bank and its HV charger, are length·width·height = 2.3·0.8·1.5 m^3 = 2.76 m^3.

A. Calculation of Dynamic Resistance and Self and Mutual Inductance

Two parallel-connected capacitors GAEP type 37331 [10], each with a capacitance of 154 nF and a self-inductance of 15 nH and capable of being charged to an initial voltage $V_0 = 50$ kV, form the bank ($C_p = 308$ nF in Fig. 1). For low-repetition rate switching ('*Switch*' in Fig. 1), a trigatron type

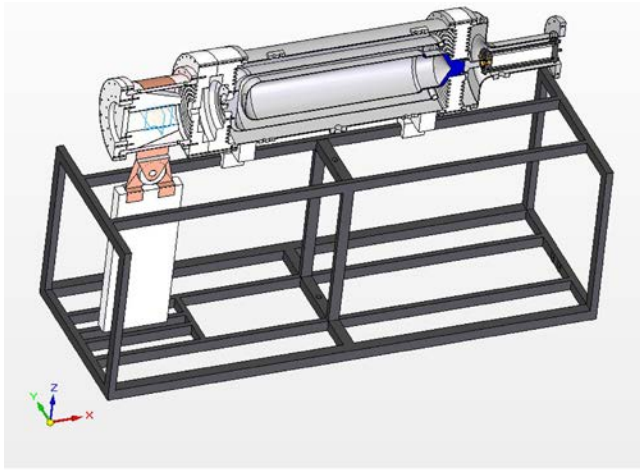




Fig. 7. (a) Overall layout of the generator mounted on a frame; (b) the completed unit

SG-101M-75C (R. E. Beverly III & Associates [11]), triggered with a trigger head pulse transformer type THD-02B-02 was used. The pulse transformer is controlled by a trigger generator type PG-103D4-02a via a 20 m fiber optic isolation link. The trigatron operates in ambient air, pressurized with N_2, between about 20 kV and 30 kV although for higher voltages it needs to be immersed in oil. The trigatron resistance R_{switch} varies with the operating voltage, from tens of mΩs at $V_0 = 20$ kV to about 1 mΩ at $V_0 = 30$ kV. The resistance also varies during a discharge but, for simplicity, this rather small effect is neglected in all numerical calculations. Preliminary testing of the primary winding circuit (Fig. 8), without the secondary winding present and undertaken at very low voltage using a low-inductance insulation breakdown closing switch [12], showed that the overall self-inductance of the bank, including the switch and a short transmission line, is about 32 nH (for simplicity omitted from Fig. 1). This enables the natural resonant frequency of the primary winding circuit to be calculated as about 449 kHz, almost equal to that of the secondary winding circuit and therefore satisfying the essential requirement of Eq. 2 for the dual resonance condition to be fulfilled. Using data from the

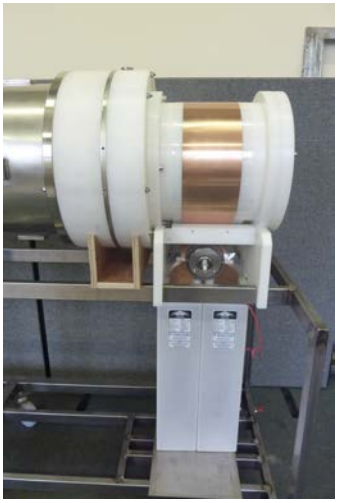


Fig. 8. Tesla transformer secondary winding

manufacturer [13], the frequency can then be used to estimate the equivalent series resistance (ESR) of the bank as $R_b \approx \frac{8}{2}\,\mathrm{m\Omega} = 4\,\mathrm{m\Omega}$ and therefore the overall resistance of the primary winding circuit as $R_p = R_{pw}^0 + R_b + R_{switch}$.

B. Blumlein Pulse Forming Line

Manufacture of the *B-PFL* 1 m long inner and intermediate electrodes is demanding, in particular the electrical grading ring attached to the intermediate electrode, which requires a precision better than 1 mm (Fig. 9) that has to be maintained after welding to the electrode. Fig. 10 shows views of mounting the *B-PFL*. Filling the cavity between the electrodes with oil is made under vacuum and is a tedious process, but after all bubbles were completely removed no breakdown issues have been encountered during more than two years of continuous usage. A self-breaking high-voltage spark-gap is used to fire the *B-PFL*. This has coaxial disc-cylinder geometry with a gap set after preliminary testing at 7.5 mm and usually operated pressurized with SF_6 to 12 bar. A small-value inductor, placed between the switch and the *B-PFL*, controls the duration of the load voltage impulse and details are provided later.

C. Load Circuit

The oil-immersed HV resistive load ($R_{load} = 30\,\Omega$) manufactured by HVR [14] comprises $N_{discs} = 12$ discs, each with an outer diameter $d_{load} = 50$ mm and a length $l_{disc} = 25.4$ mm and held under pressure by four plastic bars (Fig.11 (a)). The resistor is positioned co-axially inside a stainless steel cylinder with an inner diameter $D_{load} = 130$ mm by a Multi-Contact® connector [15] (Fig. 11(b)). As presented later, when driven by a fast rising voltage impulse, the load acts like a transmission line.

D. Diagnostics

Two high-voltage *V-dot* probes were designed following [16] (Fig. 12), manufactured and installed: one in the outer wall of the *B-PFL* and the other in the outer wall of the coaxial load.

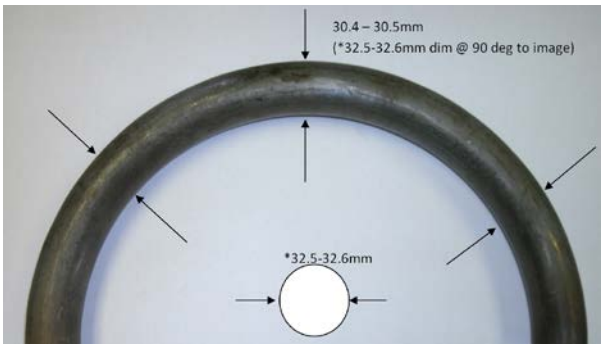


Fig. 9. *B-PFL* intermediate electrode grading ring



Fig. 10. Aspects from manufacturing and assembly
(a) outer and intermediate electrodes partially assembled
(b) inner electrode ready for mounting
(c) attaching the Tesla to the *B-PFL*

The output voltage from the *B-PFL* probe can take the form $V_{out} = C_{probe} Z_0 \frac{dV}{dt}$, where C_{probe} is the capacitance between the probe and the *B-PFL* intermediate HV electrode and $Z_0 = 50\,\Omega$ is the impedance of the signal cable connecting the

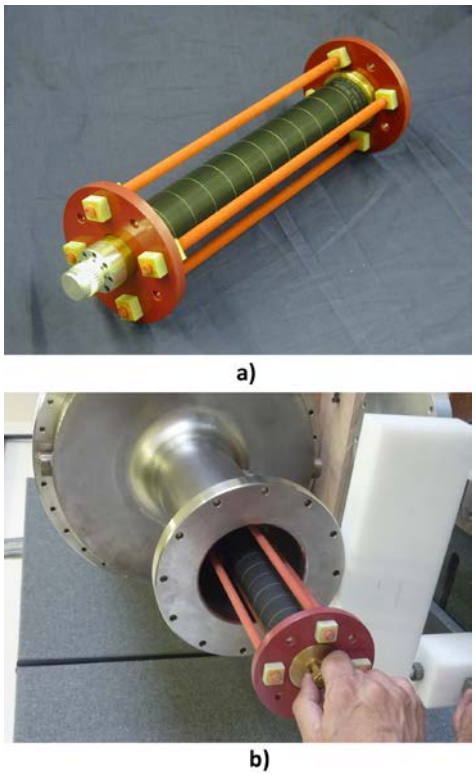


Fig. 11. 30 Ω resistive load (a) resistor showing Multi-Contact® end connector; (b) this connector allows very convenient mounting of the load

probe to an oscilloscope. The probe capacitance can be *roughly* estimated from the fraction of the *B-PFL* outer-conductor surface occupied by the probe electrode [16] as

$$C_{probe} = \frac{\varepsilon_0 \varepsilon_{oil} d^2}{r_3 ln(r_3/r_2)}$$, where $d = 20$ mm is the diameter of the probe electrode (see Figure 12a) and the *B-PFL* radii r_2 and r_3 were defined above. The estimated probe sensitivity $k_1 = C_{probe} Z_0 \approx 4.76$ ps was later accurately determined by calibration to be 5.2 ps.

Besides a similar *V-dot* probe, having a sensitivity $k_2 = 1.3$ ps, the load section also contains an *I-dot* probe [16] with numerical integration performed after the test providing all the voltage and current impulses.

E. PSpice Modeling

The PSpice model [17] of the overall system is presented in Fig. 13. From left to right it is easy to recognize the HV charging unit, followed by the bank circuit and the Tesla transformer. The *B-PFL* HV closing switch includes a series self-inductance (15 nH) and a parallel equivalent capacitance (1.6 pF). The already mentioned inductor, connecting the HV switch to the *B-PFL*, controls the load voltage impulse characteristics to meet the specific application. For a charging voltage $V_0 = 30$ kV and a 38 nH inductor, the FWHM is 15 ns and the load peak voltage close to 600 kV, and when the inductance is 20 nH or less, the FWHM is reduced to about 10 ns, with the load peak voltage increasing to 625 kV or even higher.

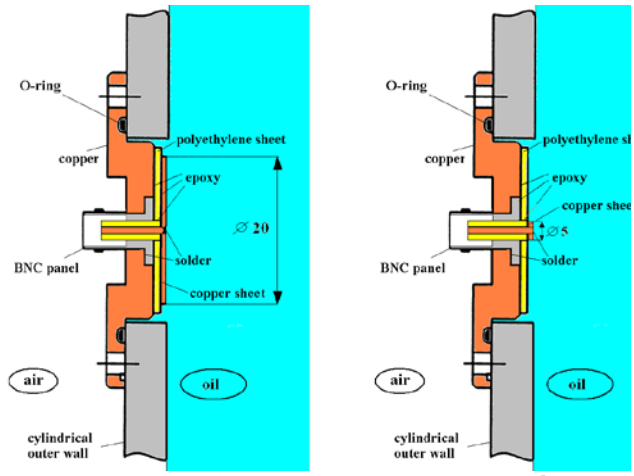


Fig. 12. Sketch of the two V-dot probe assemblies (not to scale) mounted in the outer wall of the (a) oil-filled *B-PFL*; (b) coaxial load

To the right in the PSpice model of Fig. 13 is the *B-PFL*, followed by two very short transmission lines corresponding to two transition parts, connecting the *B-PFL* to the load, while maintaining the HV integrity during charging. The load itself is modeled as a transmission line with distributed inductance, capacitance and resistance. These electrical characteristics per unit length were calculated as follows:

$$C_{T5} = \frac{2\pi\varepsilon_0\varepsilon_{oil}}{ln\left(\frac{D_{load}}{d_{load}}\right)}, \quad L_{T5} = \frac{\mu_0}{2\pi} ln\left(\frac{D_{load}}{d_{load}}\right) \text{ and } R_{T5} = \frac{R_{load}}{N_{disc} l_{disc}}$$

Finally, a small correction due to the transient skin depth effect was applied on L_{T5}.

A detailed analysis shows that, depending on the value of the primary winding circuit resistance mainly dictated by the bank closing switch, the overall energy efficiency of the Tesla transformer calculated as $\eta = \frac{C_p V_0^2}{C_s V_s^2}$ can vary between approximately 83% for $R_p \approx 60$ mΩ up to about 95% for $R_p \approx 7$ mΩ. In practice, as the *B-PFL* HV switch never closes at V_s (V_s is the peak voltage that can be generated by Tesla transformer in the secondary winding circuit for a given V_0), the actual efficiency is slightly lower.

V. Results

A. Single-Shot Operation: Investigating the Limits

In an effort to investigate the limits, at an initial bank charging voltage of $V_0 = 30$ kV, operation of the system begins with *B-PFL* being charged by the Tesla transformer for 1.4 μs, followed by the fast discharge of the *B-PFL* (Fig. 14). The record voltage impulse has a peak time rate-of-change of about 225 kV/ns (Fig. 15(a)) and an integrated peak of $V_{peak} = 596$ kV, with a rise time of 2.2 ns (Fig 15(b)). The corresponding overall Tesla transformer efficiency is in this case $\frac{C_p V_0^2}{C_s V_{peak}^2} \approx 92\%$ and, after the *B-PFL* HV switch closes,

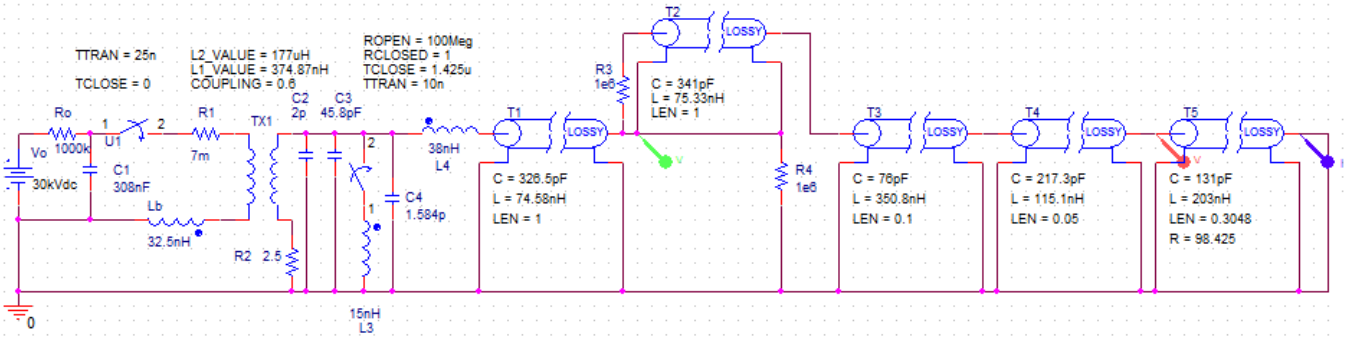
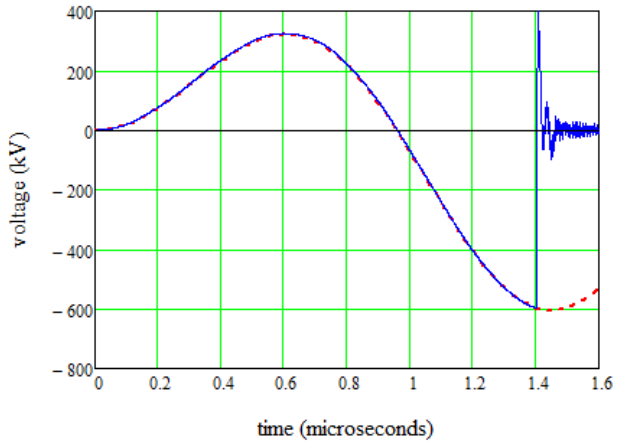
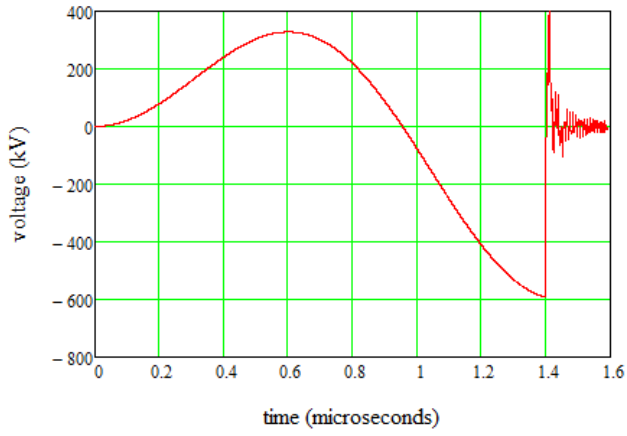


Fig. 13. PSpice model of the overall system



a)



b)

Fig. 14. Time history of *B-PFL* voltage during a 0.6 MV shot; (a) experimental data (continuous blue line) compared with 2D filamentary modeling (dotted red line) (b) PSpice prediction (very similar to experimental data). Time origin from the bank switch closure

a percentage $\frac{C_{B\text{-}PFL}}{C_s} \approx 94\%$ of the energy $\frac{C_s V_{peak}^2}{2} = 127$ J is transferred to the load with a peak instantaneous power of 10 GW (Fig. 16).

Typically however, the generator is operated at a peak load voltage close to 500 kV (Fig. 17), with an experimentally observed dispersion of the peak load voltage for five 'identical' consecutive shots being 485 kV ±3%. The corresponding peak instantaneous power is about 7 GW.

B. Repetitive Operation

Repetitive operation, in bursts of five shots, has been tested between 1 Hz and 2 Hz, with the dispersion in the load voltage being ± 8%. Flowing SF_6 gas during discharge or re-design of the spark gap will both increase the repetition rate that can be achieved and the reproducibility of the peak load voltage.

VI. CONCLUSIONS

A compact Tesla transformer has been developed and has successfully charged capacitive loads to peak voltages up to 0.6 MV with an overall energy efficiency in excess of 90%. Based on this unit, a Blumlein PFL pulsed power generator has been designed, manufactured and successfully tested. The generator is capable of producing a voltage impulse approaching 0.6 MV with a rise time close to 2 ns, generating an electrical peak power of 10 GW when connected to a 30 Ω load. Repetitive operation has been demonstrated at lower voltage and power levels.

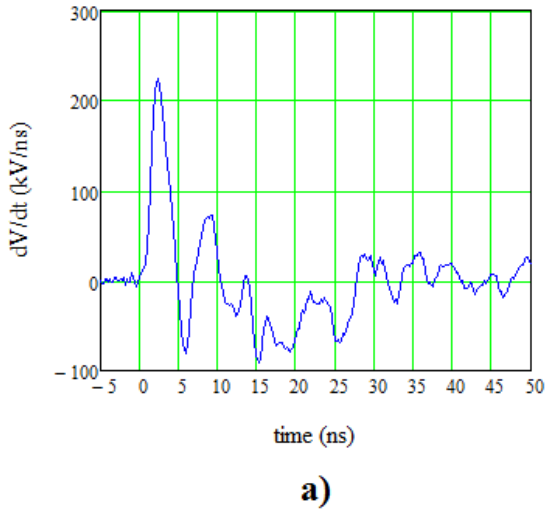
Future plans include improving the *B-PFL* HV switch operation and replacing the static, 30 Ω load resistor, with a bipolar pulse conditioning unit using techniques similar to those presented in [18-20]. Implementation of this unit, which includes a pair of very fast acting high-pressure closing switches, will reduce the rise time of the output voltage impulse to hundreds of picoseconds. In the final phase of development the pulsed power system will be connected to a more representative load.

REFERENCES

[1] W.J. Sarjeant and R.E. Dollinger, "*High-power electronics*", TAB BOOKS Inc., USA, 1989

[2] J. Luo, B. M. Novac, I. R. Smith, and J. Brown, , "Fast and accurate two dimensional modeling of high-current, high-voltage air-cored transformers", *J. Phys. D , Appl. Phys.*, vol. 38, no. 6, 2005, pp. 955–963

[3] P. Sarkar, B.M. Novac, I.R. Smith, G. Louverdis, '2D Modelling of Skin and Proximity effects in Tesla Transformers', in *Proceedings of the 2008 IEEE International Power Modulators and High Voltage Conference*, pp. 268 - 271



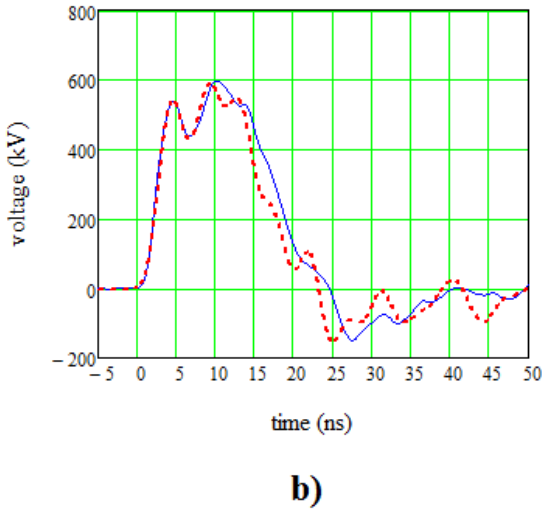


Fig. 15. Load voltage corresponding to the test of Fig. 14
(a) time rate-of-change signal
(b) integrated voltage (continuous blue line), compared with PSpice prediction (dotted red line); time origin from *B-PFL* HV switch closure

[4] A.H.M. Arnold, 'The resistance of round-wire single-layer inductance coils', *Proc. IEE*, vol.98, 1951, pp. 94-100
[5] http://www.ansoft.com/products/em/maxwell/, last time accessed in November 2013
[6] Q. Yu and T.W. Holmes, A Study on Stray Capacitance Modeling of Inductors by using the Finite Element Method, *IEEE Trans. on Electr. Comp.*, Vol. 43, 2001, pp. 88-93
[7] B.M. Novac, I.R. Smith, Meng Wang and P. Senior, 'Tesla-Charged Blumlein High-Power Generator', in *Proc. 2013 IEEE International Pulsed Power & Plasma Science Conference* (to be published)
[8] T. H Martin, A Guenther and M Kristiansen (Eds) '*J.C. Martin on pulsed power*', Plenum Press:
N.Y. and London, 1996
[9] K. Nielsen, H. Davis, E. Ballard, J. Elizondo, R. Gribble, B. McCuistian, and W. Parsons, "Atlas transmission line breakdown analysis," in *Proc. 12th IEEE Int Pulsed Power Conference*, 1999, Vol. 1, pp. 381–384.
[10] http://www.ga-esi.com/EP/capacitors/index.php, last time accessed in November 2013
[11] http://www.reb3.com/, last time accessed in November 2013
[12] P. Senior; C.D. Hackett, B.M. Novac, and I.R. Smith, 'Switch characteristics for a high efficiency 20 kJ electromagnetic launcher', in *Proc. 11th IEEE International Pulsed Power Conference*, 1997, Vol. 2, pp. 1144 - 1149
[13] GAEP, private communication

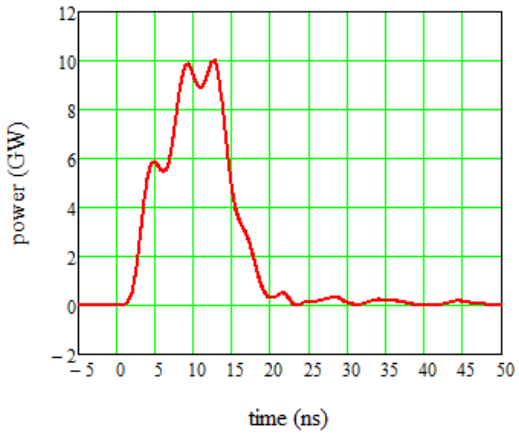
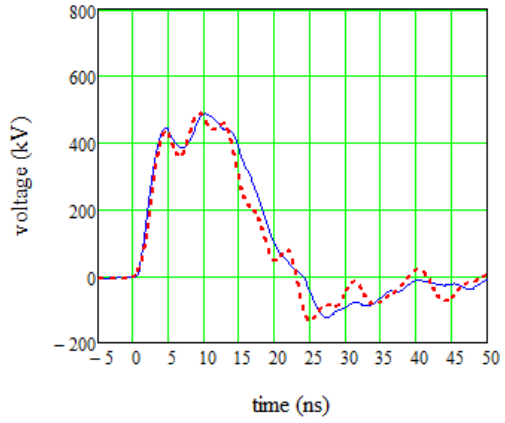


Fig. 16. Instantaneous load power corresponding to data in Figs. 14 and 15. Time origin from *B-PFL* HV switch closure



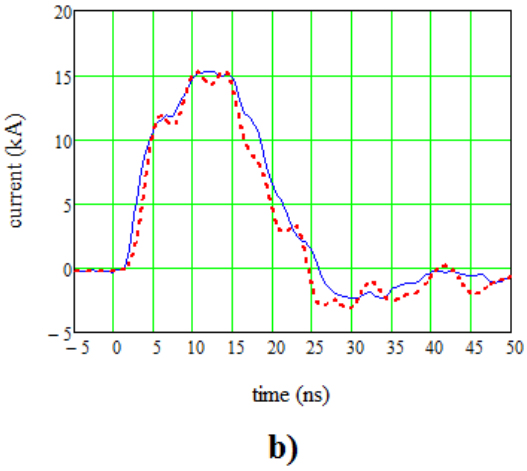


Fig. 17. Load voltage and current corresponding to a standard ≈0.5 MV test. Integrated signals (a) voltage and (b) current; experimental data (continuous blue lines) compared with PSpice prediction (dotted red lines); for convenience the current is presented as positive; time origin from *B-PFL* HV switch closure

[14] http://www.hvrint.com/, last time accessed in November 2013
[15] http://www.multi-contact.com/, last time accessed in November 2013
[16] C. A. Ekdahl, 'Voltage and current sensors for a high-density z-pinch experiment', *Rev. Sci. Instrum*. Vol. 51, pp. 1645-1648 (1980)
[17] http://www.cadence.com/products/orcad/pspice_simulation/pages/default.aspx, last time accessed in November 2013

[18] Y. A. Andreev, V. P. Gubanov, A. M. Efremov, V. I. Koshelev, S. D. Korovin, B. M. Kovalchuk, V. V. Kremnev, V. V. Plisko, A. S. Stepchenko and K. N. Sukhushin, "High-power ultrawideband radiation source", *Laser and Particle Beams*, vol. 21, no. 02, 2003, pp. 211-217
[19] V. I. Koshelev, V. P. Gubanov, A. M. Efremov, S. D. Korovin, B. M. Kovalchuk, V. V. Plisko, A. S. Stepchenko and K. N. Sukhushin, "High-power ultrawideband radiation source with multielement array antenna", *13th International Symposium in High Current Electronics*, Tomsk, 2004, pp. 258-261
[20] A. M. Efremov, V. I. Koshelev, B. M. Kovalchuk, V. V. Plisko and K. N. Sukhushin, "High-power sources of ultra-wideband radiation with subnanosecond pulse lengths", *Instruments and Experimental Techniques*, vol. 54, no. 1, 2011, pp. 70-76



Bucur M. Novac (M'06 – SM'08) received the M.Sc. and Ph.D. degrees in 1977 and 1989, respectively. He joined the Loughborough University, UK in 1998 and is currently Professor of Pulsed Power. His research interests include compact and repetitive high-power systems, explosively and electromagnetically driven magnetic flux compression generators and their applications, electromagnetic launchers, ultrafast magneto and electro-optic sensors and 2-D modeling of pulsed-power systems.
Prof. Novac is a voting member on the Pulsed Power Science & Technology Committee in the IEEE Nuclear and Plasma Science Society. He is also a member of the International Steering Committees for both the MEGAGAUSS Conferences and for the Euro-Asian Pulsed Power Conferences. He is also member of the organizing committee for the IEEE International Power Modulator and High Voltage Conference and co-chairman of the UK Pulsed Power Symposium. Prof. Novac is a Chartered Engineer and a Fellow of The Institution of Engineering and Technology (IET), UK.



Meng Wang (S'13) was born in China. She received the B.Sc. degree in Electronics Science and Technology from Huazhong University of Science and Technology, China, in 2011 and the M.Sc. degree in Power Systems Engineering from University College London, UK, in 2012. She is currently working towards the Ph.D. degree in the Pulsed Power Group, Loughborough University, UK. Her Ph.D. project is focused on the development of a 10 GW pulsed power generator. Her current research interests are in compact and repetitive pulsed power, ultrahigh speed sensors and modeling and analysis of 3D electromagnetic systems.



Ivor R. Smith (M'05-SM'11) received both B.Sc. and Ph.D. degrees from the University or Bristol, UK after completing an indentured student apprenticeship at the Witton Works of the General Electric company. He then became a Lecturer at the University of Birmingham, UK, subsequently being promoted to Senior Lecturer and Reader and being awarded the degree of D.Sc. by the University of Bristol for his continued research contribution. He then moved to Loughborough University, UK to become Professor of Electrical Power Engineering, and served as Head of Department, Dean of Engineering and Pro-Vice Chancellor. For more than 25 years he has been active in research in many aspects of the production, conditioning and utilization of large pulses of electrical energy and his work has brought in very substantial funding from a variety of sources.
Professor Smith is a Chartered Engineer and a Fellow of both the Institution of Engineering and Technology and the Royal Academy of Engineering.



Peter Senior received an Honours Degree in Physics with Electronics from Leicester University. He is a member of the Institute of Physics and a Chartered Physicist. He began his career in the Electronic and Electrical Engineering Department at Loughborough University researching Ultrasonic Nondestructive Evaluation, extending into Nonlinear (Finite Amplitude) Acoustics. He was one of the founder members of the Pulsed Power Research Group. He has worked on Propellant and Explosive Pulsed MHD Generators, and also produced systems to support a Flux Compressor Programme. Other work has included High Efficiency Launchers and the Electromagnetic Protection of Armoured Vehicles. He has produced a number of Transportable High Energy, High Power Systems, varying in size between fitting into a van, and up to two ISO Containers, supplied by diesel generators. This has required expertise in the Health and Safety Aspects of integrating Pulsed Power systems with the equipment of sponsoring and collaborating bodies.